Journal of Materials Chemistry B

ROYAL SOCIETY OF CHEMISTRY

PAPER

View Article Online
View Journal | View Issue

Cite this: J. Mater. Chem. B, 2025, 13, 11663

Enhanced therapeutic efficacy of cationic liposome-delivered nerve growth factor antisense oligonucleotide for interstitial cystitis/bladder pain syndrome

Yuan Gao, †[ab] Ying Zhao, †[ab] Lin Zhu, [c] Hanwei Ke, [c] Wenxin Li, [ab] Sulaiman Ganiu Bolaji, [ab] Huimei Wang, *[d] Kexin Xu *[c] and Lianyan Wang *[ab]

The pathogenesis of interstitial cystitis/bladder pain syndrome (IC/BPS) remains unclear, and there is no definitive treatment for this condition. Studies have shown that antisense oligonucleotide (asODN) targeting nerve growth factor (NGF) can downregulate the level of NGF in the bladder, however, the uptake of NGF asODN by the body is limited. Therefore, this study constructed cationic liposomes (CLs) as a delivery system to carry NGF asODN and evaluated its functional efficacy on the bladder. The results indicated that the optimized CLs/asODN delivery system had an average particle size of approximately 200 nm, an average zeta potential of around +53 mV, and an encapsulation efficiency of over 90% with good stability. Additionally, CLs/asODN significantly facilitated the uptake of asODN fluorescence by the urothelium, with an uptake rate of 14.6%, which was 40.2 times free asODN. In a rat model of IC/BPS, treatment with CLs/asODN reduced voiding frequency, significantly increased maximum cystometric capacity, prolonged inter-contraction interval of the bladder, and improved bladder compliance. Furthermore, hematoxylin-eosin staining and immunohistochemical analysis revealed significantly reduced expression levels of NGF, PACAP, Piezo2, CCL2, IL-6, and TGF-β factors after treatment, indicating that the overexpression of NGF in the bladder could be indirectly blocked by complexing NGF asODN with cationic liposomes. The CLs/asODN prepared in this study improved the adhesion and penetration of the drug at the bladder mucosa site, effectively alleviated bladder dysfunction in rats, and further enhanced the inhibitory effect of asODN on NGF, which may provide a new strategy for the treatment of IC/BPS.

Received 9th April 2025,
Accepted 13th August 2025

DOI: 10.1039/d5tb00820d

rsc.li/materials-b

1. Introduction

Interstitial cystitis/bladder pain syndrome (IC/BPS) is a bladder inflammatory disorder characterized by chronic bladder pain accompanied by symptoms such as increased urinary frequency, urgency, and nocturia, which significantly impairs patients' quality of life and even increases the risk of mortality.[1–3] Currently developed pharmacological treatments for IC/BPS include oral pentosan polysulfate sodium and intravesical instillations of dimethyl sulfoxide, hyaluronic acid, and lidocaine, among others.[4,5] All these methodologies aim to control the disease and provide substantial benefits to the affected patients. However, due to the complexity of the pathogenesis and etiology of IC/BPS, it remains challenging to induce significant and sustained therapeutic effects while ensuring safety. Therefore, the development of effective therapeutic strategies for IC/BPS is particularly crucial.

Studies have shown that IC/BPS can alter bladder inflammatory-related factors, such as elevated urinary nerve growth factor (NGF) levels.[6,7] NGF contributes to bladder dysfunction by mediating bladder inflammation and modulating the morphology and function of bladder afferents and sympathetic nerves.[8] Thus, urinary NGF might be a useful biomarker for the differential diagnosis of IC/PBS, and targeting NGF may represent a promising approach for improving

[a] Key Laboratory of Green Process and Engineering, State Key Laboratory of Biochemical Engineering, Institute of Process Engineering, Chinese Academy of Sciences, Beijing 100190, P. R. China. E-mail: wanglianyan@ipe.ac.cn
[b] University of the Chinese Academy of Sciences, Beijing 100049, P. R. China
[c] Department of Urology, Peking University People's Hospital, Beijing 100044, China. E-mail: cavinx@yeah.net
[d] State Key Laboratory of Subtropical Silviculture, College of Forestry and Biotechnology, Zhejiang A&F University, Hangzhou 311300, Zhejiang, China. E-mail: whm0709@163.com
† These authors contributed equally to this work and should be considered co-first authors.

IC/BPS. Antisense oligonucleotide (asODN) mechanisms, a promising method for the rational design of gene-based therapies, have undergone clinical research for over 30 years.[9] They work by using short synthetic ODNs to achieve sequence-specific gene silencing and thereby block NGF gene expression. However, the clinical application of asODN-based therapies is hindered by their susceptibility to degradation by nucleases in the environment and their low efficiency in crossing cell membranes. Consequently, there is a need for efficient and low-toxicity NGF asODN delivery vectors to enhance bladder uptake of asODNs.

In recent years, nano-drug delivery systems have been developed for the treatment of IC/BPS.[10–13] Liposomes, as widely studied nanocarriers, not only protect drugs from degradation and improve their stability but also enhance drug permeability across biological membranes and increase drug interaction with damaged urothelial cells, thereby improving therapeutic efficacy.[14–16] Using liposome delivery technology *via* intravesical instillation to locally inhibit NGF expression in the bladder may be an effective method for treating IC/BPS. While local instillation can avoid systemic adverse reactions, it also has limitations, including limited drug uptake by bladder epithelial cells. Therefore, optimizing the nanocarrier formulation and fabrication process is crucial for achieving efficient therapeutic effects.

In this study, a cationic liposome (CL) was constructed as a delivery system for NGF asODN. The preparation conditions of this delivery system were optimized, and the therapeutic effects of intravesical instillation of CLs/asODN were evaluated. The bladder uptake of CLs-asODN was studied *in vitro*. In addition, changes in rats' voiding behavior patterns and urodynamic testing were investigated to analyze improvements in bladder function. Furthermore, hematoxylin-eosin (H&E) staining was used to observe morphological changes in rat bladder tissue before and after instillation, and immunohistochemical analysis was also conducted to assess the expression levels of various inflammatory-related factors, exploring the pathological changes of IC/BPS at the molecular level.

2. Materials and methods

2.1. Materials and animals

The 18mer phosphorothioated antisense ODN was designed with the sequence 5′GCCCGAGACGCCTCCCGA3′, which was labeled by a 5′ tag of FAM by Beijing Ruibo Xingke Biotechnology Co., Ltd (Beijing, China). DOTAP and DOPE were purchased from AVT Pharmaceutical Tech Co., Ltd (Shanghai, China). Trichloromethane was obtained from Sinopharm Chemical Reagent Co., Ltd (Shanghai, China). The cell counting kit-8 (CCK-8) was supplied by Dojindo Laboratories (Kumamoto, Kyushu, Japan). Cyclophosphamide (CYP) was provided by Sigma (St. Louis, MO, USA). GAPDH was purchased from Abcam (Cambridge, UK). Anti-PACAP receptor/ADCYAP1 and Piezo2 antibodies were purchased from Novus Biologicals (Littleton, USA). Anti-NGF rabbit polyclonal antibody was provided by Thermo Fisher Scientific Inc. (Waltham, MA, USA). All other chemical reagents were of analytical grade.

SPF-grade Sprague-Dawley rats (10–11 weeks, female), with weights ranging between 250 g and 280 g, were purchased from Vital River Laboratories (Beijing, China). All the animal experiments were approved by the Animal Ethics Committee of the Institute of Process Engineering and strictly followed the Regulations for the Care and Use of Laboratory Animals and Guideline for Ethical Review of Animal (China, GB/T35892-2018).

2.2. Preparation of CLs and CLs-asODN

CLs-asODN were prepared using the thin film hydration method. DOTAP and DOPE with a molar ratio 1 : 1 were dissolved with 2 mL of chloroform. The solution was then subjected to vacuum rotary evaporation (RE-3000A, Zhenjie Laboratory Equipment Co., Ltd, Shanghai, China) at 40 °C water bath for 30 min until a thin lipid film formed on the inner wall of the flask. The flask was placed in a vacuum oven at 40 °C for 1 h to remove the organic solvent completely. Then, an appropriate volume of deionized water was added into the flask, followed by hydration through rotary evaporation at 60 °C for 1 h. After hydration, the solution was allowed to cool down to room temperature. Then, the lipid suspension was sonicated. Subsequently, a nano-extruder was used to extrude the suspension multiple times through a 200 nm pore-size polycarbonate membrane to obtain unilamellar CLs. CLs-asODN was obtained by incubating asODN (10 μM) with liposomes for 30 min at room temperature.

2.3. Characterization of CLs and CLs-asODN

2.3.1. Size, polydispersity index (PDI), and zeta potential. The size, PDI, and zeta potential of CLs and CLs-asODN were detected by dynamic light scattering (DLS) using a laser particle size analyzer (Nano ZSP, Malvern Instruments, Malvern, UK). For size and PDI, 1 mL of CLs or CLs-asODN suspension was placed in a quartz cuvette and then measured at room temperature. To measure the zeta potential, 1 mL of CLs or CLs-asODN suspension was carefully transferred into a potential sample cell, making sure no bubbles were introduced. The sample was then placed into the Nano ZSP instrument, and the measurement was initiated.

2.3.2. The morphology of CLs. The morphology of CLs was observed using transmission electron microscopy (TEM) (HT7700, Hitachi Ltd, Tokyo, Japan). A carbon-coated copper grid was placed on a parafilm-covered watch glass. Then, 10 μL of liposome suspension was dispensed onto the parafilm, and the grid was inverted onto it for 10 min to adsorb the sample. The grid was stained with 2% phosphotungstic acid for 60 s and air-dried. The labeled grid was then observed under a TEM at 120 kV to assess liposome morphology and structure.

2.3.3. Stability of CLs. The stability of CLs was evaluated by storing them at 4 °C and analyzing particle size and zeta potential on days 0, 5, 10, 15, 20, and 25.

2.3.4. The binding affinity of CLs to NGF asODN. CLs-asODN complexes with various R_4N^+/P ratios (1 : 1, 2 : 1, 4 : 1, 8 : 1, 10 : 1) were prepared and incubated at room temperature

for 30 min. Subsequently, 10 × DNA loading buffer was added and mixed. 0.3 g of agarose was dissolved in 30 mL of 1 × TAE buffer. The solution was heated in a microwave until the agarose powder was completely dissolved. After allowing it to cool slightly, 10 μL of ethidium bromide solution was added. The mixture was gently shaken to ensure uniformity, then poured into a gel tray, and a comb was inserted. The tray was left to allow the agarose gel to solidify. Next, 1 × TAE electrophoresis buffer was added to the electrophoresis chamber, and the gel was positioned with the sample wells near the negative pole. The comb was then removed, and the samples were loaded. Electrophoresis was conducted at 100 V for 1.5 h. Afterward, the gel was placed in a gel imaging system (GELDoc Go, Bio-Rad Laboratories Co., Ltd, Hercules, USA) for observation and photography.

2.3.5. Determination of encapsulation efficiency and drug loading efficiency of CLs/asODN. The encapsulation efficiency (EE) and drug loading efficiency (LE) of the CLs/asODN were determined using a reduction method. 500 μL of CLs/asODN complex with different R_4N^+/P ratios was precisely pipetted into a 30 kDa ultrafiltration tube, and centrifuged at 5000 rpm for 45 min to collect the filtrate. Then, 200 μL of the centrifuged ultrafiltrate was taken and its absorbance was measured using a Varioskan LUX microplate reader (Thermo Fisher Scientific Inc., USA) at an excitation wavelength of 492 nm and an emission wavelength of 518 nm to calculate the amount of free asODN based on the standard curve. According to the following equations, the EE and LE were calculated, respectively.

$$\mathrm{EE} = \left(\frac{M_{\mathrm{asODN}} - M_{\mathrm{free}}}{M_{\mathrm{asODN}}}\right) \times 100\% \quad (1)$$

$$\mathrm{LE} = \left(\frac{M_{\mathrm{asODN}} - M_{\mathrm{free}}}{M_{\mathrm{total}}}\right) \times 100\% \quad (2)$$

where M_{free}, M_{asODN}, and M_{total} represent the weight of free asODN, the total weight of asODN, and the total weight of asODN complexed with liposomes, respectively.

2.4. *In vitro* safety evaluation of CLs-ODN

The cytotoxicity of CLs/asODN was evaluated using the CCK-8 method. SV-HUC-1 cells were seeded into a 96-well plate at a density of 5×10^4 cells per well in a volume of 50 μL, and supplemented with 100 μL of Ham's F-12K culture medium containing 10% FBS and 1% penicillin–streptomycin. The cells were incubated at 37 °C and 5% CO_2 for 24 h. Subsequently, the cells were exposed to 50 μL of either asODN or CLs/asODN at a final concentration of 100 nM asODN, with varying R_4N^+/P ratios of 1 : 1, 2 : 1, 4 : 1, 8 : 1, and 10 : 1, and incubated for an additional 18 h. Then, 20 μL of CCK-8 reagent was added to each well, followed by gentle shaking and mixing. Negative control wells (cells and culture medium) and blank control wells (culture medium only) were established. The cells were then incubated for another 4 h, and the absorbance at 450 nm was measured using a Varioskan LUX microplate reader to determine cell viability.

2.5. Analysis of the uptake of NGF asODN by bladder urothelial cells

18 SPF-grade Sprague Dawley rats (adult, female) were divided into three groups: the control, the asODN (0.5 mL, 10 μM), and the CLs/asODN (0.5 mL, 10 μM asODN, R_4N^+/P ratio of 8) groups. The asODN was labeled with FAM. After anesthetizing the rats with 2% isoflurane, a polyethylene catheter was inserted into the bladder *via* the urethra to drain it, followed by instillation of 0.5 mL of saline, FAM-conjugated antisense ODN, or liposome complex for 45 min. Upon completion of the infusion, the rats were awakened, and a catheter clamp was placed at the urethral orifice for another 45 min before removing the clamp to allow resumption of urination. After 24 h, three rats from each group were euthanized, and their bladder tissues were sectioned into 8 μm frozen slices using a cryostat maintained at 25 °C. Two-photon microscopy (FVMPE-RS, Olympus Corporation, Japan) was employed to observe the uptake of asODN by rat bladder epithelial cells. The bladder tissues of the remaining three rats in each group were digested with collagenase to prepare single-cell suspensions and flow cytometry was used to quantify the uptake efficiency of asODN by rat bladder epithelial cells.

2.6. Development of the IC/BPS model

The intraperitoneal injection model of CYP IC/BPS was used for *in vivo* IC/BPS treatment research in rats.[17] 12 adult female SPF-grade Sprague-Dawley rats were selected and randomly divided into control and CYP treatment groups, with 6 rats in each group. As shown in Fig. 4A, rats were administered intraperitoneal injections of 1 mL CYP (75 mg kg^{-1}) on days 0, 3, and 6, while the control group received an equal volume of saline. On day 7, the rats were euthanized, and their bladders were collected. The bladders were then fixed in formalin solution, embedded in paraffin, and sectioned into 8 μm slices. These slices were stained using routine H&E staining and sealed with neutral gum. The histopathological changes in the bladder tissues of rats from each group were observed under a light microscope (Nikon Eclipse E100, Nikon Corporation, Japan).

2.7. Void spot assay (VSA)

18 rats were divided into 3 groups, including control, CYP treatment saline, and CYP treatment CLs/asODN (10 μM) groups. All the rats were moved individually to empty mouse cages with pre-cut filter paper (Whatman grade 1 qualitative filter paper, 32 × 38 cm) on the bottom. They were not provided with food and water. After 4 h, rats were treated with perfusion and replaced with new filter paper for another 4 h. Then, 36 pieces of filter papers were allowed to dry before being photographed under UV light (365 nm) in a Chromato-Vue C75 imaging box with an onboard Canon camera (EOS Rebel T3-12 megapixels). Image J and UrineQuant software were employed to analyze the number and area of void spots.

2.8. Analysis of urodynamics

Cystometrograms (CMG) were used to test the urodynamics. 30 rats were randomly divided into 5 groups (control, CYP-saline,

CYP-asODN, CYP-CLs, and CYP-CLs/asODN groups) with 6 rats in each group. Before the urodynamic test, rats were prohibited from drinking water for 12 h. After anesthesia by inhalation of 2–3% isoflurane, a 19G BD ureteral catheter was inserted into the bladder of rats and filled at a rate of 0.1 mL min^{-1}. The ureteral catheter was connected to the syringe pump and pressure sensor through a three-way stopcock. The maximum cystometric capacity (MCC), intercontraction interval (ICI), bladder compliance (BC), and detrusor pressure (Pdet) were recorded.

2.9. Immunohistochemistry

Following CMG administration, bladder tissues from each experimental group were promptly fixed with 4% paraformaldehyde post-isolation. These tissues were subsequently embedded in paraffin and sectioned to a thickness of 8 μm. Dewaxing of the paraffin sections was achieved using xylene and a gradient ethanol series. Endogenous peroxidase activity was inhibited with 3% hydrogen peroxide, followed by sequential incubation with 3% BSA, primary antibodies, and secondary antibodies (detailed in Table S1, including dilution ratios). Diaminobenzidine (DAB) was utilized to visualize the immunoreactions. Counterstaining was performed with hematoxylin, and the sections were dehydrated through an ascending alcohol series before being mounted with neutral balsam and examined under a light microscope. Additional morphological assessments were conducted using H&E staining. Fluorescent microscopy (Leica, Germany) was employed for image capture. The staining intensities of NGF, PACAP, Piezo2, CCL2, IL-6, TGF-β, IL-1β, IL-17, TNF-α, and CCL3 inflammatory markers in rat bladder tissues across all groups were quantified using the H-score system, facilitating statistical analysis of the immunohistochemical data.

$$\text{H-Score} = \sum(\text{pi} \times i) \quad (3)$$

where pi represents the percentage of positive cells in the total number of cells in the slice; i represents staining intensity, which means i represents weak (i = 1), moderate (i = 2), or strong staining (i = 3).

2.10. Statistical analysis

The results of this study were expressed as mean ± SEM and used GraphPad Prism 8.0 software for statistical analysis. One-way ANOVA was employed to determine statistical significance among mean values across different groups, with $p < 0.05$ considered indicative of significant differences.

3. Results and discussion

3.1. Optimization of CLs preparation

3.1.1. Effect of different hydration temperatures on particle size and dispersion of CLs. The hydration temperature plays a pivotal role in the formation process of liposomes, and it must exceed the phase transition temperature of the phospholipids. Because when the hydration temperature is below the phase transition temperature, liposomes remain rigid and are not easily resized through extrusion.[18] This study employed DOTAP and DOPE to prepare the liposomes, and the particle size and polydispersion index of liposomes were evaluated by DLS at a hydration temperature of 50 °C, 55 °C, 60 °C, and 65 °C. As shown in Fig. 1A, liposomes formed at 60 °C and 65 °C exhibited a particle size of ∼150 nm with excellent uniformity and dispersion. However, higher temperatures may lead to excessive oxidation of phospholipids, which may change their properties and affect the loading of asODN drug.[19] Therefore, 60 °C was selected as the optimal hydration temperature.

3.1.2. Effect of different mediums of hydration on particle size and dispersion of CLs. CLs were prepared in Tris HCl aqueous solution, 5% glucose aqueous solution, PBS buffer, and deionized water to obtain the optimal hydration mediums. And its particle size and PDI were evaluated by DLS. As shown in Fig. 1B, when PBS buffer was used as the hydration medium, the liposomes had a larger particle size, which easily induced flocculation and precipitation of the CLs suspension, hindering the formation of monodisperse CLs. The CLs obtained from the other three hydration media had particle sizes ranging from 120 to 150 nm, exhibiting good uniformity and dispersibility. The morphology of CLs using different mediums was studied by TEM. However, the morphology of CLs in Tris HCl and 5% Glucose hydration solutions was less favorable, possibly due to the disruption of the lipid membrane structure during the hydration process (Fig. 1C). Therefore, deionized water was selected as the hydration medium for the subsequent preparation study.

3.1.3. Effect of different ultrasound power on particle size and dispersion of CLs. The ultrasound phenomena occurring in liquid media facilitate the non-uniform mass transport of their constituents, thereby enabling the rapid formation of vesicles.[20] Due to the high local energy output of the ultrasonic cell pulverizer and the resulting local overheating of the liposome suspension, which can damage the lipid membrane, so ultrasonic cleaning was chosen for the preparation of CLs in the experiment. The particle size and dispersity of CLs were evaluated by DLS and compared under ultrasonic powers of 150, 300, and 450 W, with further analysis conducted on the impact of these ultrasonic powers (Fig. 1D). The results showed that the ultrasonic power increased, with a trend of decreasing particle size. This may be attributed to the influence of frequency on liposome size reduction, which correlates with the intensity of cavitation resulting from variations in bubble dynamics. Specifically, at lower frequencies, the amplitude of cavitation bubble oscillation increases, leading to more potent impulsive shock waves and microjet streams. Consequently, liposomes experience a smaller number of intense impacts when subjected to low-frequency sonication, compared to the numerous but weaker impacts of high-frequency ultrasound. Since the breakage of large liposome to make smaller ones involve plastic deformation, it is natural to consider that the small number of strong impact is favorable when the total energy is equal.[21] In addition, CLs obtained under 300 W ultrasonic power displayed good dispersity with relatively uniform. However, when the ultrasonic power was set at 150 W and 450 W, the CLs exhibited higher PDI values, leading to poorer

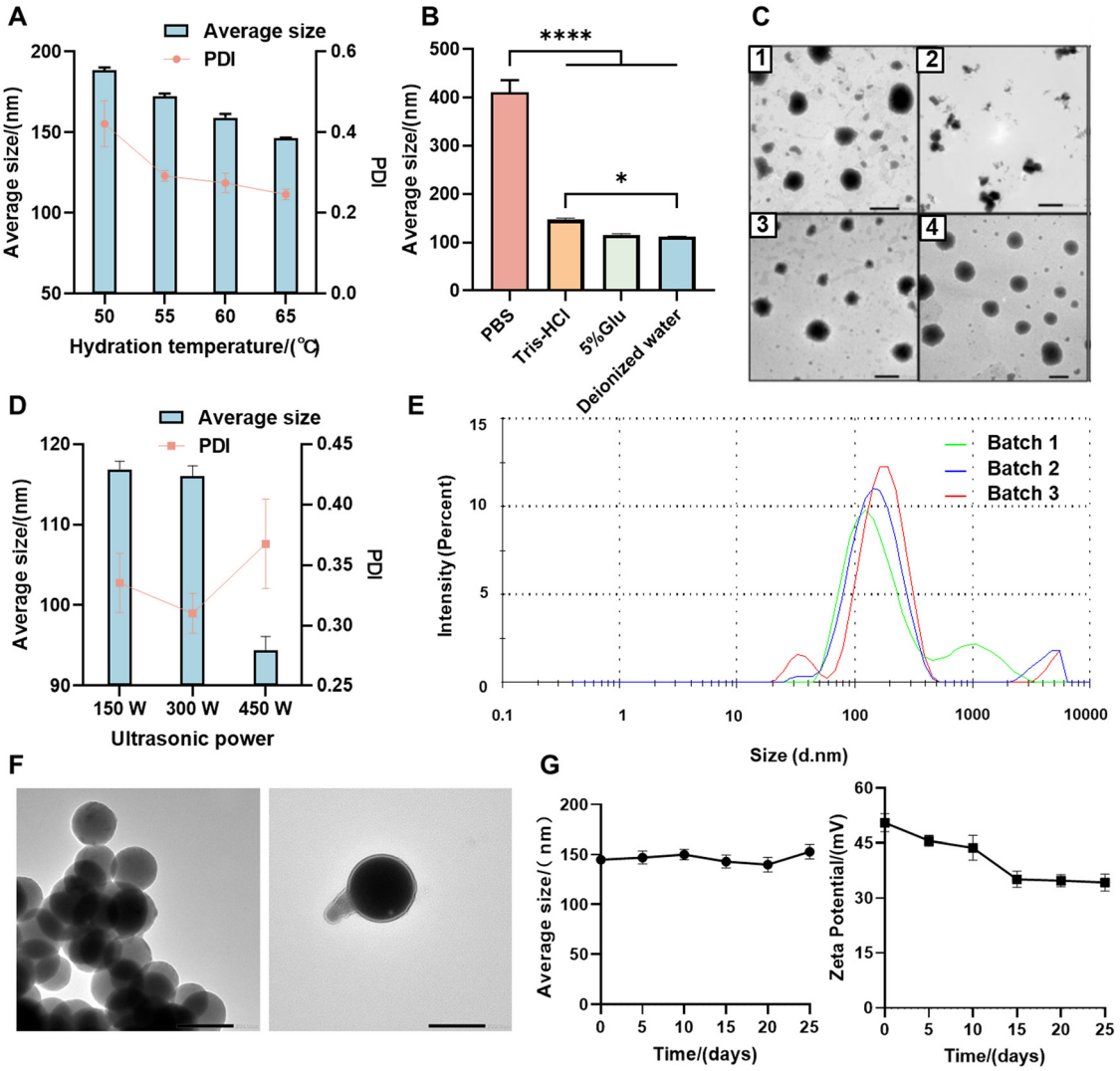

Fig. 1 Effect of preparation conditions on physicochemical properties of CLs. (A) Effect of hydration temperature on particle size and PDI of CLs, (B) effect of mediums of hydration on particle size and PDI of CLs, (C) transmission electron microscope (TEM) results of CLs: 1–4 were the different mediums of hydration of PBS Tris–HCl, 5%Glu, and deionized water groups, respectively (the scale bar in Fig. 1C1 was 500 nm, while those in all other figures were 200 nm), (D) effect of ultrasound power on particle size and PDI of CLs, (E) and (F) the particle size distribution and TEM images (bar = 200 nm) of CLs, and (G) stability of CLs in 25 days at 4 °C. *$p < 0.05$ and ****$p < 0.0001$.

dispersity and a more uneven distribution. Therefore, 300 W of ultrasonic power is suitable for preparing CLs.

3.1.4. Verification of the optimized conditions of CLs. To verify the reproducibility of the CLs preparation process, the CLs were prepared three times under the optimized conditions: the hydration temperature of liposomes of 60 °C, the hydration medium of deionized water, and the ultrasonic power of 300 W, and the results were displayed in Fig. 1E–G and Fig. S1. The DLS results indicated that the CLs exhibited a particle size of approximately 150 nm, demonstrating excellent dispersity and high reproducibility among the batches (Fig. 1E). In addition, the CLs displayed a uniform milk-white and translucent suspension. TEM imaging revealed that the CLs possessed a nearly spherical morphology and were composed of monodisperse vesicles (Fig. 1F and Fig. S1). Furthermore, the stability of the prepared CLs was evaluated in this study. Samples were collected and tested every 5 days, spanning from day 5 to day 25, under storage conditions of 4 °C. The results depicted in Fig. 1G demonstrated that the particle size of the CLs remained relatively constant over time, while the zeta potential exhibited a slight decrease but eventually stabilized. These findings suggested that CLs possess excellent reproducibility and stability, making them a suitable carrier choice for asODN.

3.2. Optimization of CLs-asODN preparation conditions

asODN molecules, characterized by their abundance of phosphate (P) groups, possess a pronounced negative charge, while the cationic liposome DOTAP bears positively charged tetraalkyl ammonium (R_4N^+) ions. Through electrostatic interactions, asODN drugs are adsorbed onto the positively charged nano-liposomes, resulting in the formation of CLs-asODN. However, an inadequate R_4N^+/P ratio can lead to problems

such as enlarged particle size, compromised stability, and incomplete encapsulation, *etc.*

As illustrated in Fig. 2A, the R_4N^+/P ratio of the CLs/asODN system was optimized, and the results showed that when the R_4N^+/P ratio ≥ 4, the particle size remained relatively constant at around 200 nm. In addition, as the R_4N^+/P ratio increased, the zeta potential transitioned from negative to positive. This transition was attributed to the decrease in asODN adsorbed onto the liposome surface when the increased R_4N^+/P ratio, significantly reduces the shielding effect on positively charged lipid components. Furthermore, when the R_4N^+/P ratio is 4 or higher, the potential remains stable, indicating that a stable state has been achieved between the cationic liposomes and asODN. To evaluate the binding of CLs to NGF asODN, agarose gel electrophoresis analysis was performed in this study. As shown in Fig. 2B, with increasing R_4N^+/P ratios, the bands gradually became darker. When the R_4N^+/P ratio was 8 : 1, no band appeared at the position corresponding to free asODN, indicating complete binding of the cationic liposomes to asODN. This observation is consistent with the trends in particle size and surface potential mentioned above. As shown in Fig. 2C, with increasing R_4N^+/P ratios, the encapsulation efficiency of the drug-loaded system also increased. When the R_4N^+/P ratio was 8, the encapsulation efficiency reached 90%. The results also indicated that at an R_4N^+/P ratio of 8, the drug loading was above 5. Therefore, based on the comprehensive evaluation of particle size, potential, and binding degree, this study selected an R_4N^+/P ratio of 8 : 1 as the optimal condition for CLs-asODN preparation.

3.3. Cell viability studies of CLs-asODN

The cytotoxicity of the various CLs-asODN was evaluated with a series of R_4N^+/P ratios of 1 : 1, 2 : 1, 4 : 1, 8 : 1, and 10 : 1. As shown in Fig. 2E, with increasing R_4N^+/P ratios, the cell viability of SV-HUC-1 cells decreased. Cationic liposomes exhibit a tendency towards enhanced membrane interaction, disrupting normal cellular functions and compromising the integrity of membranes and other subcellular compartments, ultimately leading to cellular toxicity.[22] However, when the R_4N^+/P ratio was 8, the cell viability remained above 80%. As for the viability of SV-HUC-1 cells, there were no obvious changes in the groups treated with a concentration of more than 8 : 1, indicating that the delivery system has a weak inhibitory effect on bladder epithelial cells and possesses certain biosafety.

3.4. CLs-asODN could enhance the bladder uptake

The uptake of FAM-labeled asODN in the bladder of rats was observed under a two-photon microscope. As shown in Fig. 3B, less green fluorescence entered bladder urothelial cells in the free asODN group, while a large number of green fluorescence signals were detected in the urothelial cells in the presence of liposome carriers. To further quantify the uptake efficiency of the liposomal asODN delivery system, its content was expressed as mean fluorescence intensity. In this study, rat bladder

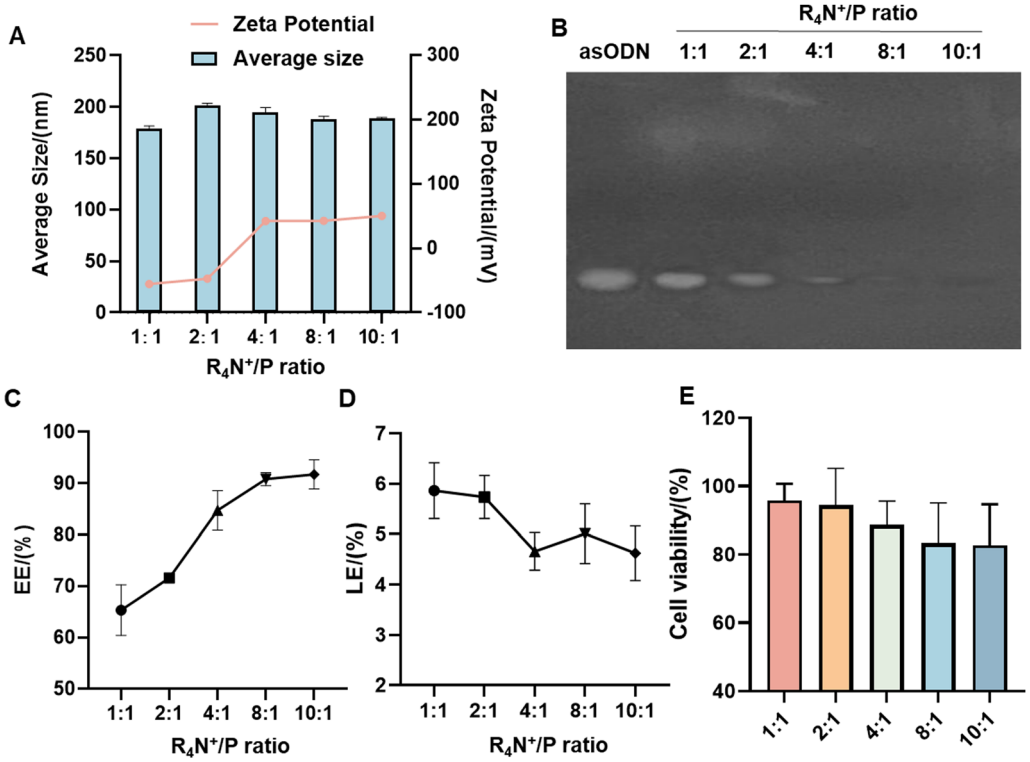

Fig. 2 Characterization of CLs/asODN under optimized conditions. (A) Effect of different R_4N^+/P ratios on the particle size and zeta potential of CLs/asODN, (B) results of CLs/asODN agarose gel electrophoresis with different R_4N^+/P ratios, (C) and (D) the encapsulation efficiency (EE) and drug loading efficiency (LE) of CLs/asODN, respectively, and (E) cell viability of CLs/asODN.

urothelial cells were digested by enzymatic digestion, and the flow cytometry results are shown in Fig. 3C. When liposome was used as a delivery vector, the fluorescence uptake efficiency of asODN by bladder urothelial cells reached 14.6%, which was significantly higher 40.2 times than that of the free asODN group. This may be attributed to the liposomes' ability to enhance cellular uptake of cationic lipids and facilitate interactions between liposomes and the cell membrane, leading to endocytosis or fusion within the cell[23,24] and the helper lipid DOPE of CLs/asODN has been demonstrated to form an inverted hexagonal structure at endosomal pH (pH 5–6), promoting its fusion with endosome membranes, leading to the release of the lipoplex into the cytoplasm.[25] In addition, CLs molecules electrostatically attracted the phosphate groups of negatively charged asODN, forming CLs/asODN complexes. These complexes entered the cells through fusion with the negatively charged cell membrane or *via* endocytosis, preventing degradation of asODN by serum nucleases. Consequently, intracellular release of asODN occurred, enabling high expression in bladder urothelial cells.

3.5. Induced IC/BPS by CYP

CYP-induced cystitis has a wide range of applications.[26–28] CYP elicits bladder toxicity through its metabolite acrolein, leading to hemorrhagic cystitis.[29] In this study, an IC/BPS animal model was established by intraperitoneal injection of 75 mg kg^{-1} CYP in rats (Fig. 4A). As shown in Fig. 4B, there were significant differences in bladder tissue morphology between rats before and after modeling. In rats with inflammation, obvious leukocyte infiltration and cellular swelling were observed, accompanied by patchy hemorrhage of the bladder mucosa, dilation, and congestion of small blood vessels, radiating towards the center of the lesion. This indicated that the established IC/BPS modeling method can effectively simulate the mucosal inflammation under cystoscopy in IC/BPS and can be used to evaluate the efficacy of intravesical drug therapy for bladder inflammation.

3.6. Infusion of CLs/asODN improved the voiding function of the bladder in rats

Bladder dysfunction significantly impacts voiding function, resulting in symptoms such as increased urination frequency, incomplete bladder emptying, urge incontinence, and dribbling.[30,31] To evaluate the therapeutic efficacy of CLs/asODN in IC/BPS, bladder function parameters were assessed using the VSOP method. Fig. 5 A demonstrated that, compared to the CYP-saline group, rats in the CYP-CLs/asODN group exhibited a marked increase in single-void volume and a trend of decreased urine spot count following infusion. Analysis of urination counts in rats revealed that, after CLs/asODN infusion, the urine spot area increased to 242.4 per square centimeters, representing a 1.96-fold increase compared to pre-treatment levels. Furthermore, the reduction in urine spot count was particularly significant in the CYP-CLs/asODN group, decreasing from 13.7 before treatment to 4.1, a reduction of 69.8% (Fig. 5B). The changes in voiding spots observed in this study of

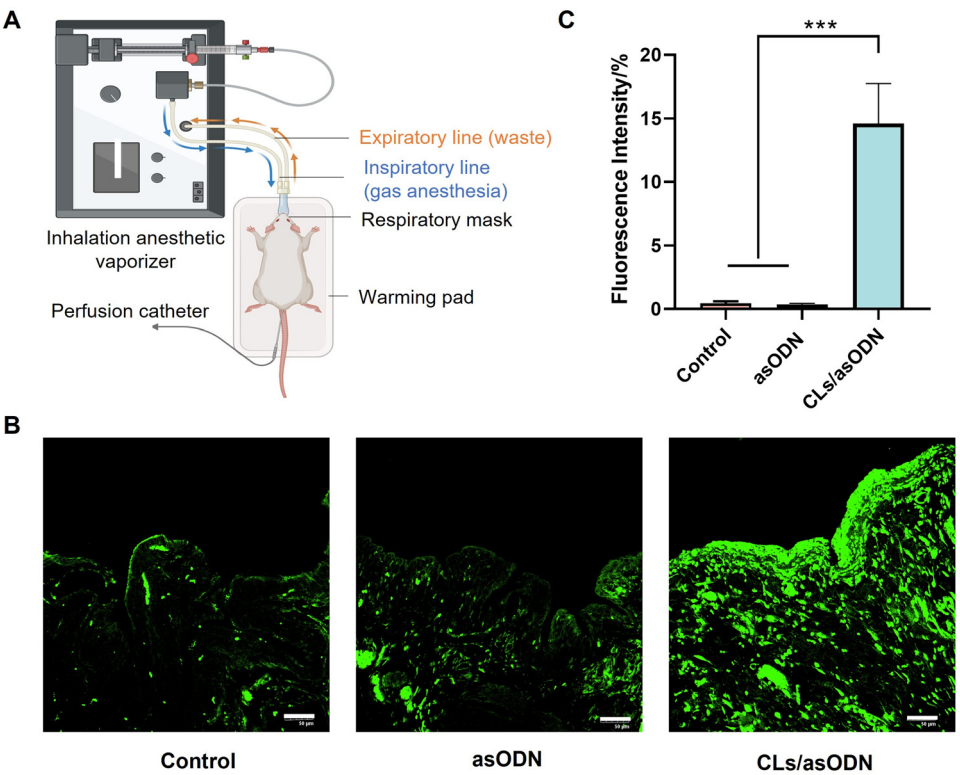

Fig. 3 Bladder uptake of CLs/asODN in rats. (A) Schematic diagram of drug infusion in rats, (B) effect of bladder uptake in rats under a two-photon microscope, harvested bladders instilled with saline, asODN, and CLs/asODN, and (C) bladder uptake efficiency after instillation of saline, asODN, and CLs/asODN treatment (bar = 50 μm). *** means $p < 0.001$.

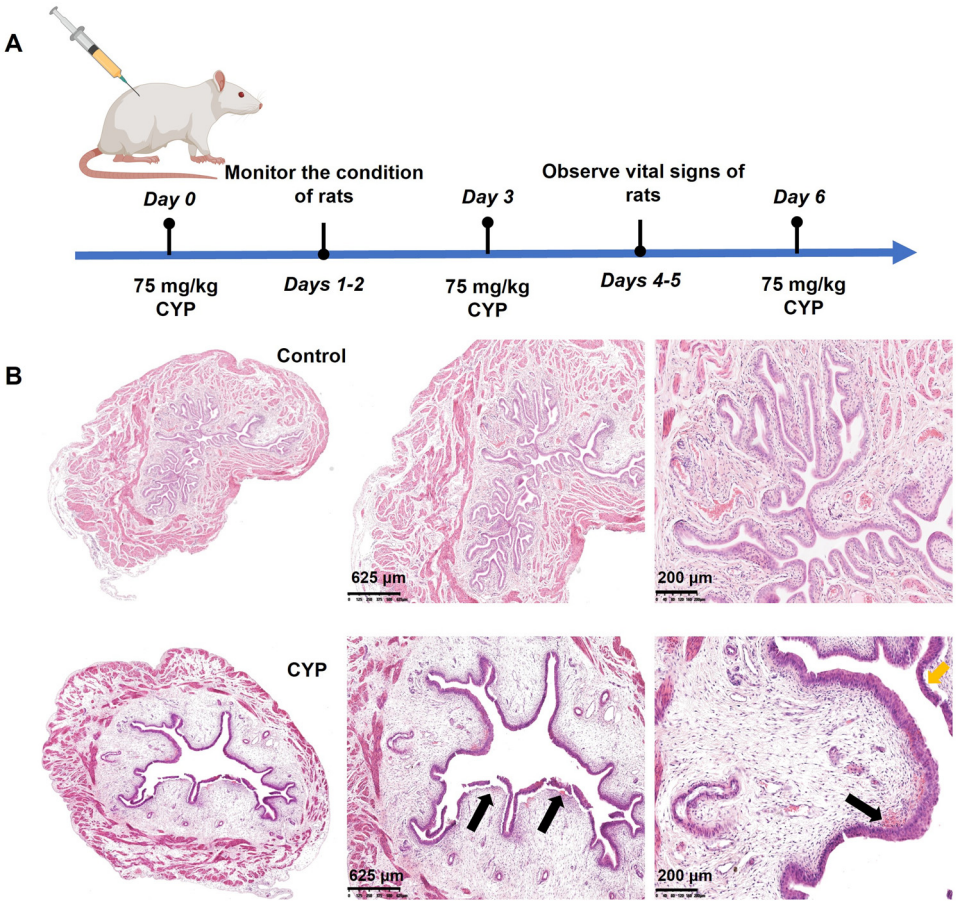

Fig. 4 Establishment of the IC/BPS model. (A) The method of establishment of IC/BPS model. (B) H&E staining of rat bladder tissue sections after injecting the 75 mg kg^{-1} CYP.

IC/BPS rats are consistent with previous research, which indicates that in mice subjected to ketamine stimulation, there is an increase in the number of voiding spots and a reduction in their size, significantly exacerbating symptoms of bladder contraction and over-activity.[32] These findings suggested that the instillation of CLs/asODN enhanced bladder capacity, decreased urinary frequency, and improved bladder dysfunction in rats.

Rats with the IC/BPS model exhibit chronic inflammatory responses, leading to alterations in bladder structure and function, which subsequently result in decreased bladder capacity and increased voiding frequency.[33] To further evaluate changes in bladder function in rats, urodynamic parameters including MCC, Pdet, ICI, and BC were measured, and the results were presented in Fig. 5C. Compared with the control group, the MCC, BC, and Pdet of the CYP-saline group were significantly decreased, indicating that the rats had bladder dysfunction after modeling. After perfusion therapy with CLs/asODN, the MCC significantly increased, while the Pdet also showed a slight elevation, but there was no statistical difference compared with other experimental groups. This may be due to the impact of anesthesia on the voiding reflex activity of the rats. Compared with the CYP-saline group, the ICI was significantly shortened in both the CYP-asODN group and the CYP-CLs group, whereas the CYP-CLs/asODN group significantly prolonged the ICI and reduced the bladder contraction frequency in rats. Furthermore, The BC in the CYP-CLs/asODN group rats was restored to nearly the control group level. The urodynamic parameter changes observed in the IC/BPS rat model are consistent with previous research which indicated the MCC Pdet, and BC of the rats in the model group were significantly lower than those in the control group.[34] Relevant clinical studies have reported urodynamic testing conducted on 171 patients with interstitial cystitis/bladder pain syndrome (IC/BPS). The research found that these patients exhibited decreased urine volume, reduced MCC levels, and increased urinary frequency. Based on the above research findings, the treatment of lower urinary tract symptoms in patients with IC/BPS is founded on the improvement of bladder urodynamics.[35] Therefore, our results indicated that perfusion with CLs/asODN can improve bladder injury, thereby enhancing bladder function in rats with the IC/BPS model.

3.7. Perfusion therapy with CLs/asODN could reduce the inflammation of bladder epithelial tissue in IC/BPS rats

Immunohistochemical staining was employed to analyze the inflammatory state of the bladder urothelium of rats following perfusion therapy, with the results presented in Fig. 6. Compared with the CYP-CLs/asODN group, an increased distribution

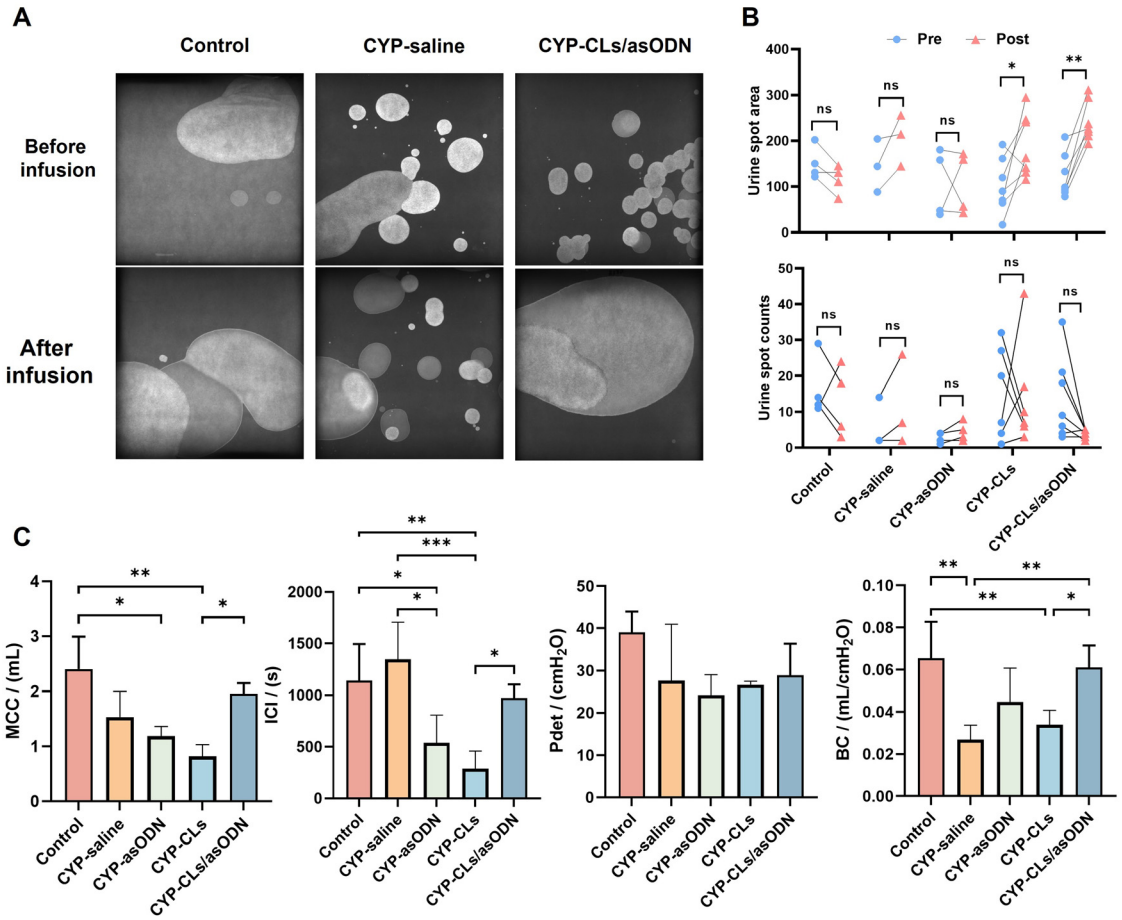

Fig. 5 Effect of perfusion therapy with CLs/asODN on urination behavior and urodynamics in IC/BPS model rats. (A) Pattern of urine spots in rats before and after treatment, (B) quantitative results of the area and count of urine spots in rats before and after treatment, and (C) evaluation of MCC, Pdet, ICI, and BC urodynamic indexes. Ns, no significance, * $p < 0.05$, ** $p < 0.01$, *** $p < 0.001$.

density of various inflammation-related factors, including NGF, PACAP, Piezo2, CCL2, IL-6, and TGF-β, was observed in the same urothelial region of the bladder in the CYP-saline group after staining. Additionally, the tight junctions between the umbrella cells of the urothelium were thinned, accompanied by deeper staining of the submucosa and the presence of significant inflammatory cell infiltration. These results suggested that perfusion with CLs/asODN exerts an inhibitory effect on the expression of these factors in the urothelium. Furthermore, the expression levels of various inflammatory factors in the tissues were quantified. NGF is recognized as a complex modulator of sensory afferent nerve plasticity in response to injury or inflammatory reactions. Elevated levels of NGF have been detected in the urine of patients with IC/BPS, suggesting that NGF may serve as a molecular biomarker for the diagnosis of IC/BPS.[36–38] From the results in Fig. 6A, the expression of NGF significantly downregulated in the CLs/asODN group compared with the CYP-saline group. However, compared with the CYP-asODN group and CYP-CLs group, there was no significant difference in the level of NGF inflammatory factors induced by CYP. In addition, the expression levels of Piezo2 and IL-6 in the CYP-CLs/asODN group were significantly decreased in contrast with those in the CYP-saline group ($p < 0.05$). It is worth noting that the liposome complex system encapsulating asODN significantly reduced the expression levels of PACAP, CCL2, and TGF-β ($p < 0.05$) compared to the single liposome group, and the expression levels of IL-1β, IL-17, TNF-α, and CCL3 in the bladder of rats treated with CLs/asODN complex were the lowest among all the experimental groups ($p < 0.05$). Piezo2 has been shown to be expressed in the urothelium and dorsal root ganglia innervating the bladder in both humans and mice, and is associated with bladder mechanotransduction, sensing the expansion of the bladder wall. Studies have reported that knocking out the Piezo2 gene significantly reduces the urothelium's response to mechanical stimulation and bladder activity.[39] Additionally, Piezo2 knockout mice exhibit symptoms such as urinary incontinence and bladder wall thickening. The chemokine CCL2 plays a role in hypersensitivity following neuronal inflammation or mechanical injury, and blocking CCL2 can reduce pain behavior caused by chronic nerve injury.[40,41] TGF-β and IL-6 are factors that regulate many aspects related to the pathology of fibrotic bladders. Relevant clinical studies have reported that urine concentrations of TGF-β and IL-6 are significantly higher in patients with bladder dysfunction compared to healthy individuals, which

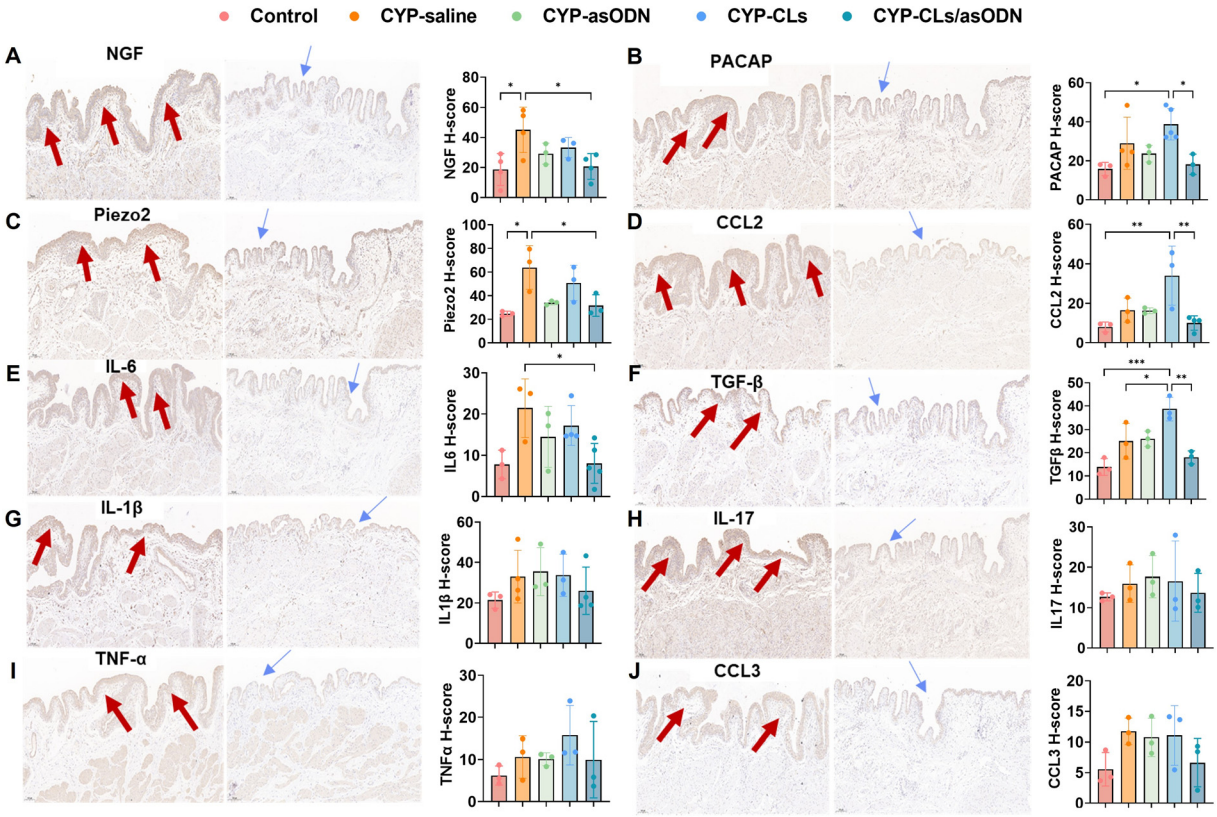

Fig. 6 Effect of perfusion therapy with CLs/asODN on the inflammation of bladder epithelial tissue in IC/BPS rats. (A–J) stand for NGF, PACAP, Piezo2, CCL2, IL-6, TGF-β, IL-1β, IL-17, TNF-α, and CCL3 respectively. Inflammatory state of bladder urothelium in rats: the left side of each factor was the CYP-saline group; the middle of each factor was the CYP-CLs/asODN group, and the right side of each factor was the expression level of inflammatory factors in rat bladder (bar = 100 μm).* $p < 0.05$, ** $p < 0.01$,*** $p < 0.001$.

may lead to inflammation-related urodynamic changes.[42,43] Consequently, these results indicated that the CLs/asODN delivery system can effectively inhibit the expression of inflammation-related factors, thereby exerting a positive effect on the treatment of IC/BPS. In addition, the overexpression of NGF in the bladder can be indirectly blocked through NGF asODN complexed with cationic liposomes. As a potential regulatory target and molecular marker of bladder function, NGF may be involved in regulating the expression levels of other inflammation-related factors. This holds significant research importance in understanding the pathogenesis and developing treatment strategies for IC/BPS disease.

4. Conclusion

In this study, CLs-asODN was successfully optimized and prepared as a novel IC/BPS therapy strategy. *In vitro* experiments confirmed that CLs-asODN had not only low toxicity but also was capable of significantly enhancing the effective uptake of the instilled drug into the cortex of the bladder urothelium. In addition, CLs-asODN could improve the lower urinary tract symptoms of functional bladder diseases. Furthermore, the overexpression of NGF in the bladder can be indirectly blocked by NGF asODN combined with cationic liposomes. This study preliminarily elucidated the therapeutic mechanism of the CL-delivered NGF asODN system at the molecular mechanism level, providing novel insights into functional liposome-mediated treatment for IC/BPS.

Author contributions

Yuan Gao: writing – original draft, methodology, formal analysis. Ying Zhao: investigation, conceptualization, data curation. Lin Zhu: methodology, data curation. Hanwei Ke: validation, visualization. Wenxin Li: investigation, validation. Sulaiman Ganiu Bolaji: software, validation. Huimei Wang: data curation, supervision. Kexin Xu: methodology, supervision. Lianyan Wang: writing – review and editing, funding acquisition, project administration, resources.

Conflicts of interest

There are no conflicts to declare.

Data availability

The data are available from the corresponding author upon reasonable request.

The supplementary information file includes the TEM image of CLs and the antibody information. See DOI: https://doi.org/10.1039/d5tb00820d

Acknowledgements

This work was financially supported by the National Natural Science Foundation of China (Grant No. 81970660, 821 71814), Beijing Natural Science Foundation (Grant No. L248068, L244079), and GuoTai (Taizhou) Center of Technology Innovation for Veterinary Biologicals Program (Grant No. GTKF(24)002).

References

1 T. Ueda, P. M. Hanno, R. Saito, J. M. Meijlink and N. Yoshimura, *Int. Neurourol. J.*, 2021, **25**, 99–110.
2 J. Li, X. Yi and J. Ai, *Int. J. Mol. Sci.*, 2022, **23**, 14594.
3 A. D. Dobberfuhl, *Neurourol. Urodynam.*, 2022, **41**, 1958–1966.
4 A. E. Dellis and A. G. Papatsoris, *Expert Opin. Pharmacother.*, 2018, **19**, 1369–1373.
5 P. Chen, W. Lee and Y. Chuang, *Expert Opin. Drug Saf.*, 2021, **20**, 1049–1059.
6 H. W. Hsiang, B. M. Girard and M. A. Vizzard, *Front. Urol.*, 2023, **2**, 1089220.
7 B. Liu, F. Yang, H. Zhan, Z. Feng, Z. Zhang, W. Li and X. Zhou, *Urol. Int.*, 2014, **92**, 202–208.
8 V. Freund-Michel and N. Frossard, *Pharmacol. Ther.*, 2008, **117**, 52–76.
9 E. Uhlmann and A. Peyman, *Chem. Rev.*, 1990, **90**, 543–584.
10 Z. Lin, B. Liu, H. Wang, H. Zhan, Y. Huang, J. Lu, Y. Tao, M. Li and X. Zhou, *Appl. Mater. Today*, 2021, **24**, 101144.
11 J. J. Janicki, M. A. Gruber and M. B. Chancellor, *Transl. Androl. Urol.*, 2015, **4**, 572–578.
12 S. Lee, J. Namgoong, H. Y. Yu, M. Jue, G. Kim, S. Jeon, D. Shin, M. Choo, J. Joo, C. Pack and J. Kim, *Nanomaterials*, 2019, **9**, 224.
13 Z. Lin, H. Hu, B. Liu, Y. Chen, Y. Tao, X. Zhou and M. Li, *J. Mater. Chem. B*, 2021, **9**, 23–34.
14 P. Tyagi, M. Kashyap, H. Hensley and N. Yoshimura, *Expert Opin. Drug Delivery*, 2016, **13**, 71–84.
15 Y. Chuang, W. Lee, W. Lee and P. Chiang, *J. Urol.*, 2009, **182**, 1393–1400.
16 T. Majima, P. Tyagi, K. Dogishi, M. Kashyap, Y. Funahashi, M. Gotoh, M. B. Chancellor and N. Yoshimura, *Hum. Gene Ther.*, 2017, **28**, 598–609.
17 B. M. Girard, S. Malley, V. May and M. A. Vizzard, *J. Mol. Neurosci.*, 2016, **59**, 531–543.
18 Z. Nemeth, E. Pallagi, D. G. Dobo, G. Kozma, Z. Konya and I. Csoka, *Pharmaceutics*, 2021, **13**, 1071.
19 R. Jangde and D. Singh, *Artif. Cells, Nanomed., Biotechnol.*, 2016, **44**, 635–641.
20 R. Silva, H. Ferreira, C. Little and A. Cavaco-Paulo, *Ultrason. Sonochem.*, 2010, **17**, 628–632.
21 T. Yamaguchi, M. Nomura, T. Matsuoka and S. Koda, *Chem. Phys. Lipids*, 2009, **160**, 58–62.
22 Y. Kumar, K. Kuche, R. Swami, S. S. Katiyar, D. Chaudhari, P. B. Katare, S. K. Banerjee and S. Jain, *Int. J. Pharm.*, 2020, **573**, 118889.
23 V. Kushwah, D. K. Jain, A. K. Agrawal and S. Jain, *Colloids Surf., B*, 2018, **172**, 213–223.
24 Z. Chen, J. Deng, Y. Zhao and T. Tao, *Int. J. Nanomed.*, 2012, **7**, 3803–3811.
25 S. Mochizuki, N. Kanegae, K. Nishina, Y. Kamikawa, K. Koiwai, H. Masunaga and K. Sakurai, *BBA-Biomembr.*, 2013, **1828**, 412–418.
26 W. Li, F. Yang, H. Zhan, B. Liu, J. Cai, Y. Luo and X. Zhou, *J. Evidence-Based Complementary Altern. Med.*, 2020, **2020**, 9026901.
27 Q. Liu, X. Li, J. Zhu, B. Sun and S. Li, *Iran. J. Basic Med. Sci.*, 2023, **26**, 701–707.
28 D. Peskar, T. Kuret, K. Lakota and A. Erman, *Int. J. Mol. Sci.*, 2023, **24**, 5758.
29 P. J. Cox, *Biochem. Pharmacol.*, 1979, **28**, 2045–2049.
30 R. Sakakibara, F. Tateno, T. Yamamoto, T. Uchiyama and T. Yamanishi, *Clin. Auton. Res.*, 2018, **28**, 83–101.
31 Q. Wang, Q. Wu, J. Wang, Y. Chen, G. Zhang, J. Chen, J. Zhao and P. Wu, *Int. J. Mol. Sci.*, 2017, **18**, 117.
32 R. Rajandram, T. A. Ong, A. H. A. Razack, B. MacIver, M. Zeidel and W. Yu, *Am. J. Physiol. Renal. Physiol.*, 2016, **310**, F885–F894.
33 C. Ryu, H. Yu, H. Lee, J. Shin, S. Lee, H. Ju, B. Paulson, S. Lee, S. Kim, J. Lim, J. Heo, K. Hong, H. Chung, J. Kim, D. Shin and M. Choo, *Theranostics*, 2018, **8**, 5610–5624.
34 F. Pan, D. Liu, X. Han, W. Li, Z. Pang, B. Li, X. Zhang, Y. Xiao and F. Zeng, *Chin. Med. J.*, 2012, **125**, 321–325.
35 A. Kim, K. Hoe, J. H. Shin and M. Choo, *Investig. Clin. Urol.*, 2017, **58**, 353–358.
36 S. Tonyali, D. Ates, F. Akbiyik, D. Kankaya, D. Baydar and A. Ergen, *Adv. Clin. Exp. Med.*, 2018, **27**, 159–163.
37 K. Duh, M. G. Funaro, W. DeGouveia, S. Bahlani, D. Pappas, S. Najjar, I. Tabansky, R. Moldwin and J. N. H. Stern, *Discovery Med.*, 2018, **25**, 243–250.
38 M. A. Vizzard, *Exp. Neurol.*, 2000, **161**, 273–284.
39 J. Ojala, K. Tooke, H. Hsiang, B. M. Girard, V. May and M. A. Vizzard, *J. Mol. Neurosci.*, 2019, **68**, 357–367.
40 J. Van Steenwinckel, A. Reaux-Le Goazigo, B. Pommier, A. Mauborgne, M.-A. Dansereau, P. Kitabgi, P. Sarret, M. Pohl and S. M. Parsadaniantz, *J. Neurosci.*, 2011, **31**, 5865–5875.
41 M.-A. Dansereau, R.-D. Gosselin, M. Pohl, B. Pommier, P. Mechighel, A. Mauborgne, W. Rostene, P. Kitabgi, N. Beaudet, P. Sarret and S. Melik-Parsadaniantz, *J. Neurochem.*, 2008, **106**, 757–769.
42 S. A. Alpert, *Int. Braz. J. Urol.*, 2009, **35**, 324–325.
43 Z. Zheng, J. Zhang, C. Zhang, W. Li, K. Ma, H. Huang, K. Li and Y. Yao, *Immun., Inflammation Dis.*, 2021, **9**, 1520–1528.